 doi:10.20944/preprints202009.0554.v1

Article

A new Retrieval of Sun-induced Chlorophyll Fluorescence in Water from Ocean Colour Measurements applied on OLCI L-1b and L-2

Lena Kritten [1]*, Rene Preusker [1] and Jürgen Fischer [1]

[1] Freie Universität Berlin
* Correspondence: lena.kritten@wew.fu-berlin.de

Abstract: The retrieval of sun-induced chlorophyll fluorescence is greatly beneficial to studies of marine phytoplankton biomass, physiology, and composition and is required for user applications and services. Customarily phytoplankton chlorophyll fluorescence is determined from satellite measurements through a fluorescence line-height algorithm using three bands around 680 nm. We propose here a modified retrieval, making use of all available bands in the relevant wavelength range with the goal to improve the effectiveness of the algorithm in optically complex waters. For the Ocean and Land Colour Instrument (OLCI) we quantify a Fluorescence Peak Height from fitting a Gaussian function and related terms into the top-of-atmosphere reflectance bands between 650 and 750 nm. This algorithm retrieves, what we call Fluorescence Peak Height from fitting a Gaussian function upon other terms to top-of-atmosphere reflectance bands between 650 and 750 nm. This approach is applicable to Level-1 and Level-2 data. We find a good correlation of the retrieved fluorescence product to global in-situ chlorophyll measurements, as well as a consistent relation between chlorophyll concentration and fluorescence from radiative transfer modelling and OLCI/in-situ comparison. The algorithm is applicable to complex waters without needing an atmospheric correction and vicarious calibration and features an inherent correction of small spectral shifts, as required for OLCI measurements.

Keywords: Remote Sensing; Ocean Colour; Retrievals; Fluorescence; Optical Properties, Satellite, Spectral, Radiative Transfer, optically complex waters, chlorophyll, absorption, scattering

1. Introduction

Chlorophyll fluorescence is light re-emitted by chlorophyll molecules when returning from excited to non-excited states. Quantification of solar-induced phytoplankton fluorescence has two main advantages in marine bio-geochemistry applications ([1,2]). These are, 1) the improvement of the chlorophyll retrieval, and 2) additional information on phytoplankton physiological state, biomass and maximum layer depth. The chlorophyll retrieval is customarily based on the detection of the chlorophyll absorption signal ([3–5]) can be gained through the ratio of the chlorophyll fluorescence to the absorption signal ([6]). Remotely sensed Fluorescence Line Height (FLH, see also eq. 1) can better reveal blooms in coastal areas than chlorophyll retrievals based on the ratios of water-leaving radiances in the blue and green spectral range (440–560 nm) by allowing better differentiation of phytoplankton chlorophyll-a concentrations from suspended sediments and yellow matter ([7]).

The pure fluorescence signal does not only vary with variation in the chlorophyll-a pigment concentration, but is also affected by photoinhibition, phytoplankton species, and physiological states ([8,9]), and layering of phytoplankton. Lin *et al.* [10] reports a strong diel cycle in in-situ measured

Preprints (www.preprints.org) | NOT PEER-REVIEWED | Posted: 23 September 2020 doi:10.20944/preprints202009.0554.v1

fluorescence lifetimes (which has a strong positive correlation to fluorescence efficiency), where the lifetimes are higher at night than during daytime.

One of the major design goals of the Medium Resolution Imaging Spectrometer (MERIS) was the capability to measure the signal of the chlorophyll fluorescence stimulated by ambient sunlight to improve the phytoplankton observation. The use of chlorophyll fluorescence was considered to be especially useful in coastal waters. Based on a variety of studies, the three spectral channels centred at 665, 681.25 and 705 nm were included in the design of MERIS for retrieving the fluorescence signal.

Using Radiative Transfer Modelling (RTM), Fischer and Kronfeld [11] stated the sun-stimulated natural fluorescence of chlorophyll-a as a good predictor for phytoplankton, even in optically complex waters with varying suspended matter and yellow substance concentrations. They found an increase in fluorescence of about 0.05 $mWm^{-2}sr^{-1}nm^{-1}$ caused by an increase in chlorophyll concentration of 1 mg/m^3, when a fluorescence efficiency factor of 0.3% was assumed. They also quantified the effect of vertical stratification.

As of now, the most established fluorescence product, which is operationally available is the Fluorescence Line Height (FLH) ([12–14]). There, a baseline is first formed by a linear interpolation of two baseline bands, and then subtracted from the radiance of the fluorescence band to obtain the FLH. The equation reads:

$$FLH = L_F - L_L - (L_R - L_L)(\lambda_F - \lambda_L)/(\lambda_R - \lambda_L) \quad (1)$$

where λ_F, λ_L, λ_R are the center wavelengths of the fluorescence band and the two baseline bands. L_F, L_L, L_R are the radiances of the fluorescence band and the two baseline bands. For MERIS, the common band combination is λ_F = 681 nm, λ_L = 665 nm, λ_R = 709 nm. For MODIS, it is λ_F = 678 nm, λ_L = 667 nm, λ_R = 748 nm. For MODIS, the standard algorithm returns the normalized Fluorescence Line Height (nFLH) in $mWcm^{-2}\mu m^{-1}sr^{-1}$, which is based on the normalized water-leaving radiance (L_w^N). Here, normalization implies the application of a Bidirectional Reflectance Distribution Function (BRDF) correction. The relation between L_w^N and ρ_w is the following [15]:

$$\rho_w^N = \frac{\pi}{F_0} L_w^N = \frac{R/R_0 * \rho_w(\theta_S, \theta_V, \phi)}{cos(\theta_S) * t(\theta_S)} \quad (2)$$

Where θ_S, θ_V and ϕ are the sun zenith angle, the viewing zenith angle and the azimuth angle respectively. While $\rho_w(\theta_S, \theta_V, \phi)$ can have different values for each combination of angles, ρ_w^N is per definition ρ_w at θ_S=0 and θ_V=0. Alternative algorithms use a simple reflectance ratio of the reflectance peak around 685 nm, e.g. reflectance at 670 and 560 nm [4]. Fluorescence products are customarily given in the unit of the processed quantity, because they measure the height or amplitude of the fluorescence peak in the measured spectrum.

A number of studies investigated the performance of FLH compared to chlorophyll absorption approaches in different regions. Hoge *et al.* [16] conducted a validation of Terra-MODIS FLH using airborne laser-induced phytoplankton chlorophyll fluorescence data retrievals within Gulf Stream, continental slope, shelf, and coastal waters of the western North Atlantic Ocean. They derived a correlation coefficient of r^2 = 0.85 and conclude that the FLH is equally valid within similar oceanic provinces of the global oceans. Huot *et al.* [17] discussed important sources of variability in sun-induced chlorophyll fluorescence, such as incident radiance, species composition and nutritional status, and examine difficulties in deriving fluorescence data products from satellite imagery. According to their findings MODIS FLH can be related to the total flux being emitted by fluorescence. Moreno-Madriñán and Fischer [18] investigated the performance of the MODIS FLH algorithm in estuarine waters and derived no overall relationships between in-situ chlorophyll-a and the FLH product (r^2=0.20,n=507). Nevertheless, the optained weak relationship was still eight times stronger than that between in-situ chlorophyll-a and the standard product OC3M [19] traditionally used to estimate chlorophyll-a in ocean waters.

 doi:10.20944/preprints202009.0554.v1

Gower and King [13] validated FLH from MERIS on the west coast of Canada. They presented an average relation between FLH and surface chlorophyll concentration from research cruises and from the blue to green ratio observed by MERIS based on a simple model accounting for absorption of stimulating and emitted radiation by chlorophyll pigments, which gives a good fit to the observations. Their results show a difference between the FLH-chlorophyll-relation for offshore waters and those in coastal straits and inlets, which is in agreement with the findings of Gons *et al.* [20], who documented the effective use of the MERIS FLH product in oligotrophic waters of the Laurentian Great Lakes, but fail (with FLH diminishing and becoming negative) in mesotrophic and eutrophic waters.

Overall, we can conclude that operational FLH algorithms that are based on the measurements of reflectance at three wavelengths in and around the fluorescence band, are sufficient for fluorescence retrieval in the open ocean where atmospheric correction algorithms work well and elastic reflectance in the fluorescence band is well approximated by the baseline curve due to the relatively weak elastic scattering signal which depends on chlorophyll alone ([21]). However, this is not the case in coastal areas. FLH products in coastal waters are significantly affected by a peak in the underlying elastic reflectance which spectrally overlaps and disturbs any fluorescence retrieval (see figure 1 for visualization). The shape and magnitude of this near-infrared peak is the result of a modulation of the particulate elastic spectrum (from both algal and non algal particles) by the combined phytoplankton and water absorption spectra. The confluence of the decreasing phytoplankton absorption and the increasing absorption of water with wavelength results in a local absorption minimum. This absorption minimum leads to the maximum in the reflectance spectra which is inversely related to the total absorption.

Binding *et al.* [22] even reported a moderate negative relationship ($R^2 = 0.57$) between FLH and in-situ chlorophyll at Lake of the Woods with chlorophyll concentration ranging between 2 - 70 mg/m^3. As a reason they suggested that at this intensity of a bloom the absorption signal of chlorophyll dominates in the 681 nm band leading to a negative FLH. Consequently, Ioannou *et al.* [23] conclude that in order to improve the operational FLH algorithms for coastal waters and compensate for the effects of the overlap of fluorescence, absorption and scattering, suitable models must be developed. Such models can take the larger impact of the spectral variation of the underlying elastic reflectance peak into account and relate the ratio of the elastic reflectance components at 667 and 678 nm to that at 488 and 547 nm. In that way, the new algorithms would improve the performance in the quantification of chlorophyll in coastal waters compared to the standard FLH algorithms.

The variability in fluorescence quantum yield caused by taxonomic differences, phytoplankton physiology and light exposure history ([21,24]) is resulting in an additional complexity of the relationship between chlorophyll-a and FLH. Nonetheless, Hu *et al.* [25] established a robust relationship between MODIS FLH and in-situ chlorophyll-a in the west Florida Shelf waters, that yielded superior estimates of chlorophyll-a compared with standard SeaWiFS or MODIS band-ratio chlorophyll-a. They were able to use FLH to differentiate between dark features on enhanced RGB images produced by high chlorophyll-a and those produced by high CDOM.

Recently, methods were developed to detect chlorophyll fluorescence in water from hyperspectral satellite measurements. Wolanin *et al.* [26] uses the filling-in of Fraunhofer lines in order to detect fluorescence from SCIAMACHY measurements. Erickson et al. [27] on the contrary, use the shape of the fluorescence peak for the retrieval of a fluorescence efficiency profile from TROPOMI. However, existing hyperspectral satellite data generally suffers from poor spatial resolution and signal-to-noise ratio.

The Earth observation satellites Sentinel-3A and Sentinel 3B both carrying the Ocean and Land Colour Instrument (OLCI) on board were launched in February 2016 and April 2018, respectively. The primary mission of OLCI is the observation of the spectral distribution of upwelling radiance just above the sea surface (the water-leaving radiance) which is then used to estimate geophysical parameters through the application of bio-optical algorithms. OLCI spectral bands are optimised to measure ocean colour over the open ocean and coastal zones. A band at 673 nm has been added

Preprints (www.preprints.org) | NOT PEER-REVIEWED | Posted: 23 September 2020 doi:10.20944/preprints202009.0554.v1

to better capture the chlorophyll fluorescence peak. Yet, no algorithm takes full advantage of the improved spectral capacities of OLCI for the detection of fluorescence.

The aim of this paper is the introduction of a new fluorescence algorithm (OC-Fluo), that makes use of OLCI's enhanced spectral capabilities in order to allow the retrieval of fluorescence even in optically complex waters. The physical principles are presented as well as the technical implementation. Finally the product is evaluated by comparing the algorithm results with in-situ measured chlorophyll concentration, OLCI's standard chlorophyll concentration, FLH from MODIS and through Radiative Transfer Modelling (RTM).

2. The OC-Fluo Algorithm

In-water chlorophyll Fluorescence is unique in its spectral shape and restriction to a distinct and narrow wavelength range. Other inherent optical properties (IOP's) in the water have comparably flat spectral features. Also, the predominant fraction of the atmospheric influence is spectrally flat (for the influence of ozone and water vapour see Section 2.5. Solely chlorophyll absorption induces another narrow spectral feature in the vicinity of the fluorescence peak. The presented algorithm utilizes the fact that chlorophyll causes the only spectrally high varying features in the 650-750 nm spectral range and allows us to be independent of absolute values and therefor of atmospheric correction. We limit the analysis to this spectral range and apply a simple curve fit to the measurements. Two Gaussian functions of defined width and spectral position capture chlorophyll absorption and fluorescence, while all other optical influences, are covered by an offset and a slope.

Consequently, both, Level-1B and Level-2 data can be processed by the OC-Fluo algorithm. It is specifically developed for OLCI measurements, but the methodology can be adapted to different sensors that measure in sufficient spectral resolution in the spectral region around the fluorescence peak. At least four bands are required, covering the chlorophyll absorption dip and the fluorescence peak between 650 and 750 nm.

Due to the uniqueness of the spectral appearance of fluorescence the algorithm should improve the retrieval in optically complex waters, where current algorithms often fail. This failure is in many cases initiated by a failure of the atmospheric correction, where e.g. an erroneous black pixel assumption leads to an overestimation of the aerosol reflectance and underestimated or negative water reflectance values in the blue bands [28]. For those cases the Level-1 fluorescence product may be still reliable. For OLCI Level-2 reflectances the following Water Quality Science Flags (WQSF) are applied: INVALID, LAND, CLOUD [29]. The algorithm does not flag negative values of ρ_w, since the algorithm can give reasonable results also with negative ρ_w, when the spectral shape of the data is preserved. Here, we apply the OC-FLuo algorithm on OLCI Level-1B top of atmosphere (TOA) radiances and Level-2 water remote sensing reflectance (Rrs) at bands 8-12 see Section 3).

2.1. Theoretical Description

The physical basis of the presented algorithm is the Lambert-Beer law, which describes extinction of electromagnetic radiation by matter.

$$I = I_0 e^{-\sigma_i(\lambda) n_i L} \tag{3}$$

Here, I_0 is incoming and I is outgoing intensity. σ_i is the attenuation cross section of the attenuating species i in the material sample; n_i is the number density of the attenuating species i in the material sample; L is the path length of the beam of light through the material sample. The equation can also be written as

$$\sigma(\lambda) nL = log(I_0/I) \tag{4}$$

In atmospheric remote sensing it is common to use the DOAS (Differential Optical Absorption Spectroscopy, [30]) approach, where the individual absorption cross sections of trace gases are fitted to the logarithm of I/I_0. Since each atmospheric trace gas has it's unique spectral finger print it is

Preprints (www.preprints.org) | NOT PEER-REVIEWED | Posted: 23 September 2020 doi:10.20944/preprints202009.0554.v1

possible to mathematically separate them. The same is valid for chlorophyll fluorescence with its unique spectral shape. The IOPs of the major water constituents as they are implemented in the RTM MOMO ([31], see also Section 3.4) are shown in figure 1: Chlorophyll fluorescence, which is an elastic process and can be modelled by a Gaussian curved source of radiation in radiative transfer, chlorophyll absorption, described by a measured absorption spectrum, detritus and CDOM absorption, both represented by an exponential decay with different slopes and scattering on particles is assumed as an spectrally inverse function. For the Fluorescence retrieval we use a simplified version of eq. 4, because the light path of the photons throughout the complete wavelength range of interest is similar. We either use radiance ($\sim I$) or reflectance ($\sim I/I_0$). This is done under the assumption that the spectral features, which are extracted by the retrieval, are induced only by the water body.

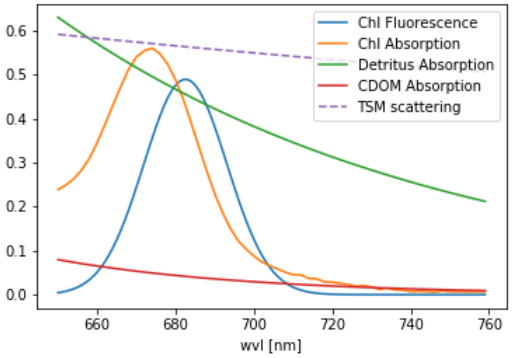

Figure 1. Optical properties of water constituents considered in the retrieval. Note, that this is only an example magnitude of the different properties.

The nomenclature we are using here for the retrieval follows the conventions given in Rodgers [32]. In short:

- $\vec{x}$ expresses the state vector, which includes the parameters to be retrieved.
- $\vec{y}$ expresses the measurement vector, which includes the measurements.
- F_{mod} is the forward model, which describes $\vec{y}$ as a function of $\vec{x}$

$$F_{mod}(\lambda, \vec{x}) = \vec{y}(\lambda) \tag{5}$$

The measured radiance or reflectance (the equation only expresses radiance for clarity) is described as:

$$L_{TOA}(\lambda) = O + S \cdot \lambda + APD \cdot exp((\lambda - \lambda_A)^2/w_A) + FPH \cdot exp((\lambda - \lambda_F)^2/w_F), \tag{6}$$

which is a function of 4 unknown (state) parameters:

- O = offset, accounting for atmospheric and oceanic scattering processes
- S = slope gradient, accounting for atmospheric and oceanic scattering processes and absorption
- APD = amplitude of Gaussian function at λ_A (absorption minimum of chlorophyll)
- FPH = amplitude of Gaussian function at λ_F (chlorophyll fluorescence peak)

and 4 fixed model parameters:

- λ_A = center wavelength of the Gaussian absorption maximum of chlorophyll in the red = 673.5 nm
- λ_F = center wavelength of the Gaussian fluorescence maximum of chlorophyll = 682.5 nm
- $w_F = 2c_F^2 = 416\,nm^2$, with c_F being the standard deviation of the Gaussian fluorescence of chlorophyll
- $w_A = 2c_A^2 = 250\,nm^2$, with c_A being the standard deviation of the Gaussian absorption of chlorophyll

(for the components see Figure 2):
The unknown parameter FPH in eq. 6 defines the fluorescence product.

Preprints (www.preprints.org) | NOT PEER-REVIEWED | Posted: 23 September 2020 doi:10.20944/preprints202009.0554.v1

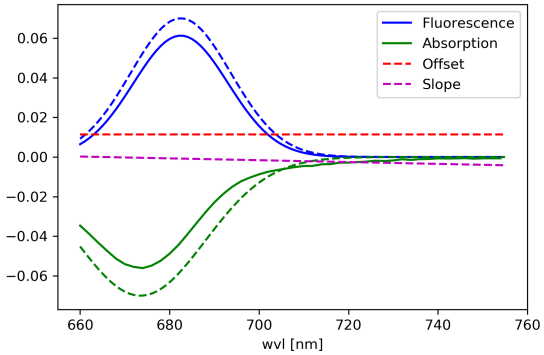

Figure 2. Components of the curve, that is fitted to the radiance spectrum.

2.2. Technical Description

Given the definitions above, the measurement vector y is given by OLCI data band 8-12 and the state x is defined by the factor for fluorescence (FPH), absorption (APD), a slope (S) and an offset (O).

$$measurement = \vec{y} = \begin{pmatrix} Oa08\_reflectance \\ Oa09\_reflectance \\ Oa10\_reflectance \\ Oa11\_reflectance \\ Oa12\_reflectance \end{pmatrix} \tag{7}$$

$$state = \vec{x} = \begin{pmatrix} O \\ S \\ APD \\ FPH \end{pmatrix} \tag{8}$$

The Jacobian is the derivative matrix of the measurement to the state. Each line of this matrix is the derivative of the forward function to the corresponding state parameter.

$$\mathbf{K} = \begin{pmatrix} \partial y_1/\partial x_1 & \partial y_2/\partial x_1 & \partial y_3/\partial x_1 & \partial y_4/\partial x_1 & \partial y_5/\partial x_1 \\ \partial y_1/\partial x_2 & \partial y_2/\partial x_2 & \partial y_3/\partial x_2 & \partial y_4/\partial x_2 & \partial y_5/\partial x_2 \\ \partial y_1/\partial x_3 & \partial y_2/\partial x_3 & \partial y_3/\partial x_1 & \partial y_4/\partial x_3 & \partial y_5/\partial x_3 \\ \partial y_1/\partial x_4 & \partial y_2/\partial x_4 & \partial y_3/\partial x_4 & \partial y_4/\partial x_4 & \partial y_5/\partial x_4 \end{pmatrix} \tag{9}$$

and therefore:

$$\vec{y} = \mathbf{K}\vec{x} \tag{10}$$

Inserting Eq. 6 gives:

$$\mathbf{K} = \begin{pmatrix} 1 & 1 & 1 & 1 & 1 \\ (\lambda_8 - \lambda_S)/1000. & (\lambda_9 - \lambda_S)/1000. & (\lambda_{10} - \lambda_S)/1000. & (\lambda_{11} - \lambda_S)/1000. & (\lambda_{12} - \lambda_S)/1000. \\ exp((\lambda_8 - \lambda_A)^2/w_A & exp((\lambda_9 - \lambda_A)^2/w_A & exp((\lambda_{10} - \lambda_A)^2/w_A & exp((\lambda_{11} - \lambda_A)^2/w_A & exp((\lambda_{12} - \lambda_A)^2/w_A \\ exp((\lambda_8 - \lambda_F)^2/w_F & exp((\lambda_9 - \lambda_F)^2/w_F & exp((\lambda_{10} - \lambda_F)^2/w_F & exp((\lambda_{11} - \lambda_F)^2/w_F & exp((\lambda_{12} - \lambda_F)^2/w_F \end{pmatrix} \tag{11}$$

For the application of this algorithm to OLCI measurements $\lambda_8 - \lambda_{12}$ are given by the nominal wavelength of band Oa8-12 (665.0 nm, 673.75 nm, 681.25 nm, 708.75 nm, 753.75 nm). In order to keep computation time low, we assume this values to be constant (for the correction of small spectral shifts see Section 2.4). Inserting the values for λ_F, λ_A, w_F and w_A gives:

Preprints (www.preprints.org) | NOT PEER-REVIEWED | Posted: 23 September 2020 doi:10.20944/preprints202009.0554.v1

$$\mathbf{K} = \begin{pmatrix} 1 & 1 & 1 & 1 & 1 \\ 0 & 8.8 \cdot 10^{-3} & 1.63 \cdot 10^{-2} & 4.38 \cdot 10^{-2} & 8.88 \cdot 10^{-2} \\ -8.4 \cdot 10^{-1} & -1 & -8.7 \cdot 10^{-1} & -5.04 \cdot 10^{-2} & -1.89 \cdot 10^{-7} \\ 2.94 \cdot 10^{-1} & 7.36 \cdot 10^{-1} & 9.94 \cdot 10^{-1} & 6.35 \cdot 10^{-2} & 1.52 \cdot 10^{-9} \end{pmatrix} \tag{12}$$

$\mathbf{K}$ is a rectangle matrix with full row rank and thus features a right inverse $\mathbf{K}_R^{-1} = \mathbf{K}^{\mathbf{T}}(\mathbf{K}\mathbf{K}^{\mathbf{T}})^{-1}$, so that the state vector $\vec{x}$ can be derived from:

$$\vec{x} = \mathbf{K}_R^{-1}\vec{y} \tag{13}$$

In principle, the number of channels that are included in the measurement vector is flexible and can be adapted according to the sensor. The number of measurements (bands) must be equal or larger than the number of state parameters to be retrieved in order to get a K-matrix that is invertable. However, including λ_A, λ_F, w_F, w_A (see equation 6) as additional parameters, makes the problem non-linear. A non-linear inversion problem can be solved in defining it locally linear, but then a number of iterations has to be performed, with an iteratively changing K, which is also different for each pixel.

$$\vec{x}_{i+1} = \vec{x}_i + \mathbf{K_{R,i}}^{-1}(\vec{y} - F(\vec{x}_i)) \tag{14}$$

The approach could also be expanded to an optimal estimation approach, which includes apriori knowledge about the state. Here measurement and apriori knowledge are weighted by their particular covariance matrices.

$$\vec{x} = (\mathbf{K}^T\mathbf{S_e}^{-1}\mathbf{K})^{-1}(\mathbf{K}^T\mathbf{S_e}^{-1}\vec{y} + \mathbf{S_a}^{-1}\vec{x_a}) \tag{15}$$

where $\mathbf{S_e}$ is the measurement covariance matrix, $\mathbf{S_a}$ the apriori covariance matrix and $\vec{x_a}$ the apriori state. The approach we are presenting her is the simplest special case of the possibilities above and most promising at this stage for OLCI measurements, but in future, when having either more knowlegde about fluorescene in water (apriori knowledge) or with hyperspectral measurements (more possible retrieval parameters) the above mentioned equation could be of value.

L-FPH is the amplitude of the Gaussian function, which is related to the fluorescence peak (centered at 682.5 nm) that is fitted to Level-1 radiance (L_{TOA}). It is therefore a measure of the fluorescence signal in the TOA radiance spectrum without any normalization. L-FPH is given in units of $mWm^{-2}sr^{-1}nm^{-1}$. ρ_w-FPH is the amplitude of the Gaussian function, which is related to the fluorescence peak (centered at 682.5 nm) that is fitted to Level-2 water-leaving reflectance (ρ_w). It is therefore a measure of the fluorescence signal in the water-leaving reflectance which is normalized by irradiance. Operational OLCI Level-2 products are defined as the directional water surface reflectance, ρ_w-FPH is dimensionless. The OLCI Level-2 products include the corrections to the water reflectance value with the Sun at zenith, the mean Earth-Sun distance, and non-attenuating atmosphere. They do not include the BRDF corrections for viewing geometry, water optical properties, and the sky radiance distribution.

2.3. Spectral Solar Irradiance (F_0) Weighting for L-FPH

The spectral distribution of the solar irradiance is known and the seasonally corrected In-band solar irradiance ($F_0(\lambda)$) is delivered with Level-1 OLCI data. In order to compensate for spectral structures introduced by F_0 that could interfere with optical properties of chlorophyll, the preprocessing for the retrieval of L-FPH includes a rectification with a normalised $F_0(\lambda)$. In practice L_{TOA} are divided by $F_0(\lambda)$ and multiplied by F_0 in band 682 nm.

$$L^*_{TOA}(\lambda) = L_{TOA}(\lambda)/F_0(\lambda) * F_0(682nm) \tag{16}$$

Preprints (www.preprints.org) | NOT PEER-REVIEWED | Posted: 23 September 2020 doi:10.20944/preprints202009.0554.v1

Input	Bands	Processing Level	Description	Output	Description	Unit
L_{TOA}	Oa08-Oa12	Level-1B	spectral top-of-atmosphere radiance	L-FPH / L-APD	radiance Fluorescence Peak Height / radiance absorption peak depth	$mWm^{-2}sr^{-1}nm^{-1}$
ρ_w	Oa08-Oa12	Level-2	water-leaving reflectance / Surface directional reflectance, corrected for atmospheric attenuation, the Sun illumination geometry, and the mean Earth-Sun distance.	ρ_w-FPH / ρ_w-APD	water-leaving reflectance Fluorescence Peak Height / water-leaving reflectance absorption peak depth	-

Table 1. In- and output description of the OC-Fluo algorithm.

2.4. The Correction of Small Spectral Shifts (Smile) for L-FPH

OLCI consists of five optical cameras, of which each exhibits a variation of the relative spectral response of the bands across the field of view, called a smile effect. This variation is further different for each module [33]. The camera to camera variations in the central spectral wavelength as well as additional small variations in each detector array are visible as stripes across swath. Those variations, up to 1.5 nm are hardly visible when looking at the whole spectral range, but they can be important when spectrally narrow features are measured with spectrally narrow channels. Accordingly the stripes can be visible in the results from algorithms assuming measurements at nominal wavelength as it is the case for the presented algorithm. Level-1 data is delivered including the central wavelength for each pixel. Operationally Level-2 data is smile corrected assuming a linear relationship between Rayleigh corrected reflectances in neighbouring bands [29]. With this assumption the water reflectances are corrected to the values as if they were measured at nominal wavelengths. We developed and implemented a smile correction for Level-1b data for band Oa08 - Oa12. The internal OC-Fluo smile correction is based on the relationship between neighbouring bands defined by Eq. 6, therefore it begins technically with the application of the retrieval (equation 13) on Level-1b data ($\vec{y_{sh}}$) measured at λ_{sh} (the subscript *sh* denotes the shifted measures).

$$\vec{x_{sh}} = \mathbf{K}_R^{-1}\vec{y_{sh}} \tag{17}$$

With the resulting state $\vec{x}_{sh}$. Assuming that the forward modelled spectrum based on $\vec{x}_{sh}$ represents the slope from measured to nominal wavelength, the change in radiance units can be calculated from the shift in wavelength through F_{mod}:

$$\Delta L_{TOA}(\lambda) = F(\lambda, \vec{x_{sh}}) - F(\lambda_{sh}, \vec{x_{sh}}) \tag{18}$$

This ΔL_{TOA} is then added to the measured L^*_{TOA}.

$$L_{TOA,corr}(\lambda) = L^*_{TOA}(\lambda) + \Delta L_{TOA}(\lambda) \tag{19}$$

$L_{TOA,corr}(\lambda)$ is now input to the retrieval. As an example for the effectiveness of this smile correction, Figure 3 shows a detail of the Barents Sea scene (Figure 7), which is also used for evaluation (see Section 3) with L-FPH, which was smile corrected by our retrieval and ρ_w-FPH, where the boundary of two cameras is still visible despite of the Level-2 smile correction.

Preprints (www.preprints.org) | NOT PEER-REVIEWED | Posted: 23 September 2020 doi:10.20944/preprints202009.0554.v1

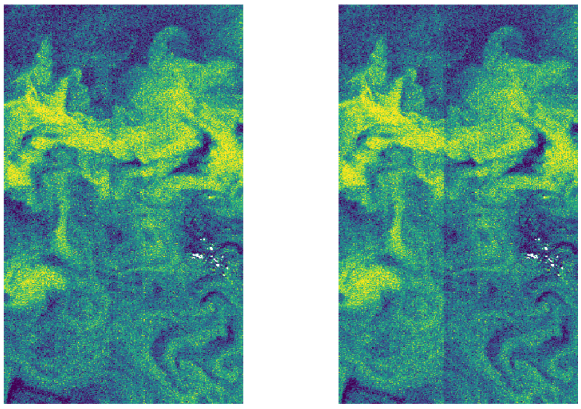

Figure 3. Comparison of the internal smile correction on Level-1b data and the standard smile correction of OLCI Level-2 data, through the comparison of the two different products in a detail of the Barents Sea scene (Figure 7) with L-FPH (left panel) and ρ_w-FPH (right panel), where the boundary of two cameras is visible in the ρ_w-FPH but not in the L-FPH.

2.5. Uncertainty with Respect to Trace Gas Absorption in L-FPH

The assumption of a spectrally flat atmospheric influence in the respective wavelength range is not valid when considering trace gases. Water vapour, ozone and nitrogen dioxide are absorbing trace gases with a non-flat spectral signature. A trace gas absorption correction is complex due to the dependency on and interaction between the trace gas vertical profile and the light path of the measured radiance and is not yet implemented in the OC-Fluo algorithm. In order to quantify the uncertainty in the L-FPH product caused by the neglect of this absorption we calculate the transmission of the respective gases based on [34]. For this example total column NO_2 is set to 2.5 molec/cm^2, ozone to 300 DU and water vapor ranges between 0 to 4 g/cm^2. After multiplying the transmission on synthetic spectra (for RTM see section 3.4), the L-FPH without and with transmission correction at an upper limit is retrieved. The difference between both (ΔL-FPH) is mainly driven by the concentration of water vapour and ranges from -0.2 in high latitudes up to 0.4 L-FPH in the tropics. In mid-latitudes the difference is only around 0.02 L-FPH. The spatial variation of water vapor is very low above open ocean and higher in coastal regions, but generally lower compared to the spatial variation of chlorophyll. Hence neglecting trace gas absorption will cause a regional offset in most cases and not modify the spatial structures in the retrieved L-FPH. Nevertheless time series and global assessments will be influenced by a varying water vapor therefore a further development of the algorithm will include a correction for water vapor (and ozone).

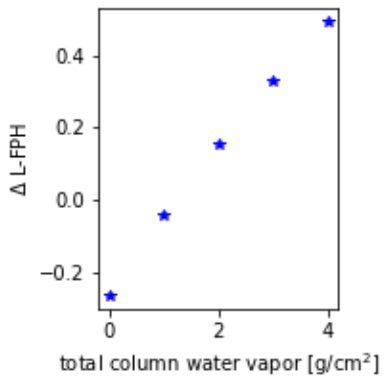

Figure 4. Difference in L-FPH without and with transmission correction over a global range of total column water vapor applied on synthetic spectra.

Preprints (www.preprints.org) | NOT PEER-REVIEWED | Posted: 23 September 2020 doi:10.20944/preprints202009.0554.v1

3. Results and Evaluation of the Algorithm

Fluorescence is a complex measure because it is not a property of the water body alone (an Inherent optical property, like e.g. chlorophyll absorption), but also a property of current and historical illumination. We cannot rely on a fluorescence ground truth for the evaluation, since in-situ fluorescence measurements are governed by active light pulses and therefor not comparable to sun-induced fluorescence. The comparison to chlorophyll is state-of-the-art for the evaluation of fluorescence algorithms (see section 1). The fluorescence is expected in first order to be correlated to chlorophyll concentration. Following these consideration, we investigate the value of our processor by the comparison to 1. in-situ chlorophyll measurements, 2. standard OLCI chlorophyll products OC4me ([35]) and NN ([36]), 3. the MODIS nFLH product and 4. results from RTM.

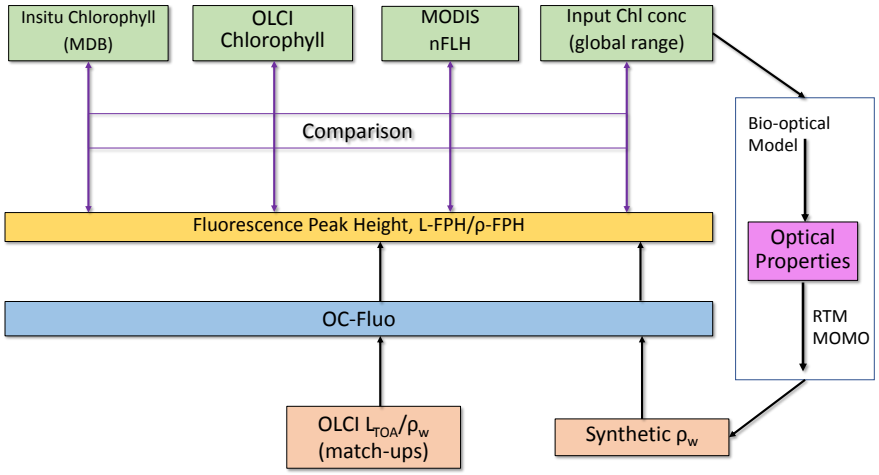

Figure 5. Evaluation of the OC-Fluo algorithm based on in-situ chlorophyll measurements, standard OLCI chlorophyll products, the MODIS nFLH product and an end-to-end simulation including RTM.

3.1. FPH against In-Situ Chlorophyll

As it is a common practice for the evaluation of remote sensing products, the main part is performed through the comparison to in-situ measurements of the same quantity. In this case the most closely related quantity is the chlorophyll concentration. For this in-situ matchup comparison the chlorophyll concentration is the result of HPLC measurements. The data is extracted from the HPLC Matchup Database which includes HPLC data from NASA SeaBASS [37] with OLCI matchups and is available at https://ocdb.eumetsat.int/ [38]. The HPLC Matchups DataBase is distributed by a netCDF file, providing both OLCI data (25 x 25 pixel centred over in-situ coordinates) and in-situ data. All variables are included as they are in the original OLCI Level-2 products. HPLC measurements are optically weighted to provide a unique value when multiple casts are provided within a radius of 150 m within 1 hour from the first measurement below the surface. A $\pm$3h window is assigned around the satellite overpass as condition for coincidence. Only in-situ measurements are included which have at least one measurement in the top layer available. For the satellite matchups, we follow the OLCI matchup protocol [39]. A box of 5x5 pixels is defined, centered on the location of the in-situ measurement. This box allows the generation of simple statistics, such as the mean and standard deviation, to assist in the evaluation of spatial stability, or homogeneity, at the evaluation point. On a pixel basis we applied the suggested Level-2 WQSF flags: CLOUD, CLOUDAMBIGUOUS, CLOUDMARGIN, INVALID, COSMETIC, SATURATED, SUSPECT, HISOLZEN, HIGHGLINT, SNOWICE, ACFAIL, WHITECAPS, ANNOTABSOD, ANNOTMIXR1, ANNOTTAU06, RWNEGO2, RWNEGO3, RWNEGO4, RWNEGO5, RWNEGO6, RWNEGO7, RWNEGO8, OC4MeFAIL. Only measurements are included where the sensor zenith is lower than 60° and the sun zenith is lower

Preprints (www.preprints.org) | NOT PEER-REVIEWED | Posted: 23 September 2020 doi:10.20944/preprints202009.0554.v1

than 70°. Most of the matchups are located in Santa Barbara Gulf in California . Thus they are not representative for all kinds of waters, but they are very well distributed throughout seasons providing examples of different levels of chlorophyll-a concentration (magenta triangle in Figure 6).

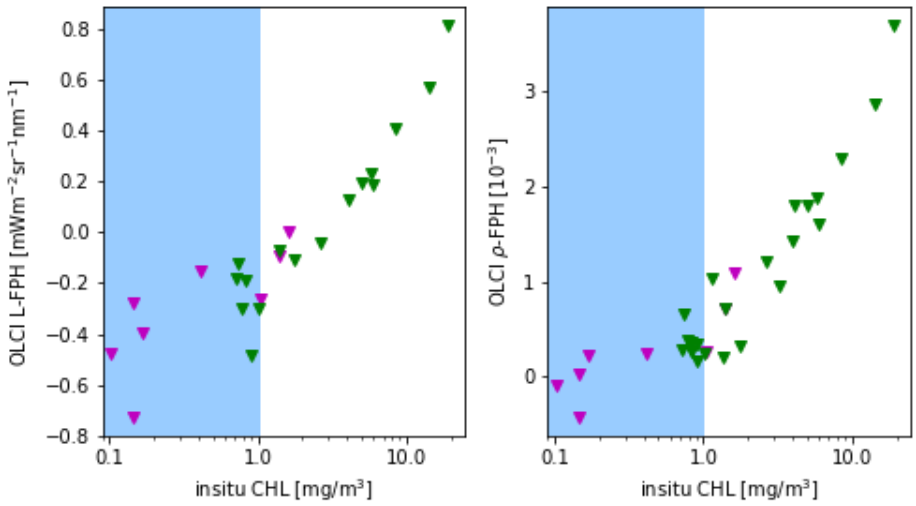

Figure 6. L-FPH from OLCI matchups over in-situ chlorophyll concentration from HPLC measurements (left panel) and ρ_w-FPH from OLCI matchups over in-situ chlorophyll concentration from HPLC measurements (right panel) from global measurements. The white background shows the proposed sensitivity range.

Figure 6 shows the retrieved ρ_w-FPH and L-FPH from OLCI matchups over in-situ chlorophyll concentration from global measurements. As well L-FPH as ρ_w-FPH from OLCI matchups show a good correlation to global in-situ measured chlorophyll, when the chlorophyll concentration is higher than $1\,\mathrm{mg/m^3}$. L-FPH obtain negative values for low chlorophyll concentration, which is most probably a negative offset due to atmospheric spectral influence. Because of the large scatter and negative values in FPH for a chlorophyll concentration roughly lower than $1\,\mathrm{mg/m^3}$, we define the sensitivity range of the algorithm above this limit, which is white in Figure 6.

Preprints (www.preprints.org) | NOT PEER-REVIEWED | Posted: 23 September 2020 doi:10.20944/preprints202009.0554.v1

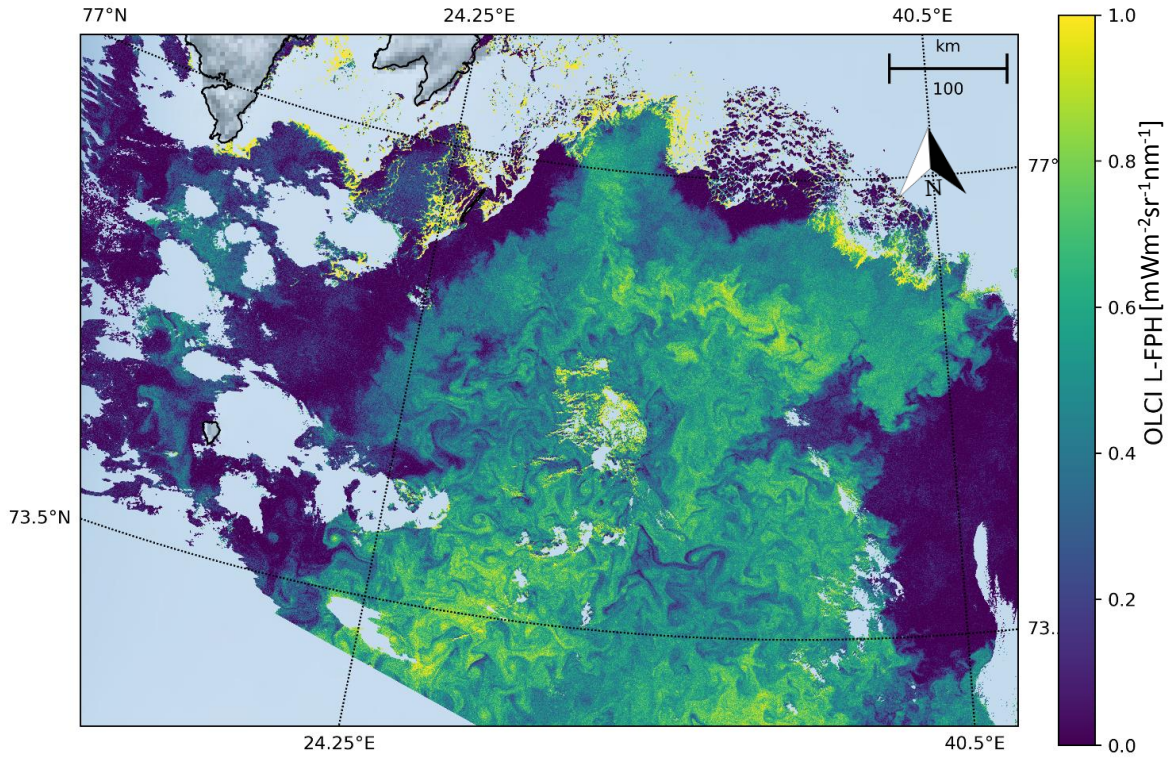

Figure 7. L-FPH from OLCI on the 7th of May, 2018 in the Barents Sea.

3.2. FPH against OLCI Level-2 Chlorophyll

Additionally, L-FPH and ρ_w-FPH are correlated to chlorophyll from the two standard operational Level-2 chlorophyll processors for OLCI, Neural Network (NN) and OC4me. In this section we compare L-FPH and ρ-FPH to chlorophyll retrieved from the Neural Network and OC4me processor by means of two example scenes with different water types. The NN chlorophyll is estimated through an Inverse Radiative Transfer Model-Neural Network approach. Here the normalised water-leaving reflectance at OLCI bands and among others the log10 of the absorption coefficient of algal pigment is estimated, from which Chl NN is derived [36]. OC4Me is a Maximum Band Ratio semi-analytical algorithm, developed by [35]. For the comparison it is important to note, that OC4Me is only appropriate in open ocean waters. Both measures are part of the operational OLCI Level-2 products.

The Barents Sea is a marginal sea of the Arctic Ocean, located off the northern coasts of Norway and Russia and is divided between Norwegian and Russian territorial waters. It is a rather shallow shelf sea, with an average depth of 230 metres, and is an important site for both fishing and hydrocarbon exploration. Despite being part of the Arctic Ocean, the Barents Sea has been characterised as "turning into the Atlantic" because of its status as "the Arctic warming hot spot." Hydrologic changes due to global warming have led to a reduction in sea ice and in stratification of the water column, which could lead to major changes in weather in Eurasia. Due to the North Atlantic drift, the Barents Sea has a high biological production compared to other oceans of similar latitude. The spring bloom of phytoplankton can start quite early close to the ice edge, because the fresh water from the melting ice makes up a stable water layer on top of the sea water. Figure 7 shows the L-FPH in the Barents Sea on the 7th of May, 2018, with only the processors default flags (see Section 2) applied, apparently revealing nice swirling and filamentary patterns of ocean chlorophyll.

The comparison of L-FPH and ρ_w-FPH to chlorophyll from OC4Me and NN in the Barents Sea is shown in Figure 8. For this pixel-wise comparison the OLCI matchup protocol [39] is applied. There is a clear correlation between both fluorescence and both chlorophyll concentration measures. For chlorophyll > $1\text{mg}/\text{m}^3$ the correlation gets stronger in both cases

Preprints (www.preprints.org) | NOT PEER-REVIEWED | Posted: 23 September 2020 doi:10.20944/preprints202009.0554.v1

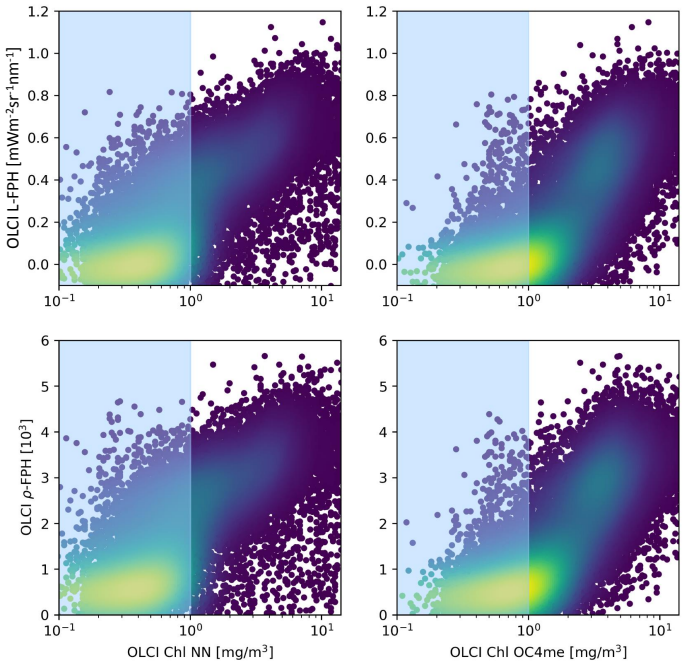

Figure 8. L-FPH and ρ_w-FPH against chlorophyll from OC4me (upper panel) and against chlorophyll from NN in the Barents Sea.

Preprints (www.preprints.org) | NOT PEER-REVIEWED | Posted: 23 September 2020 doi:10.20944/preprints202009.0554.v1

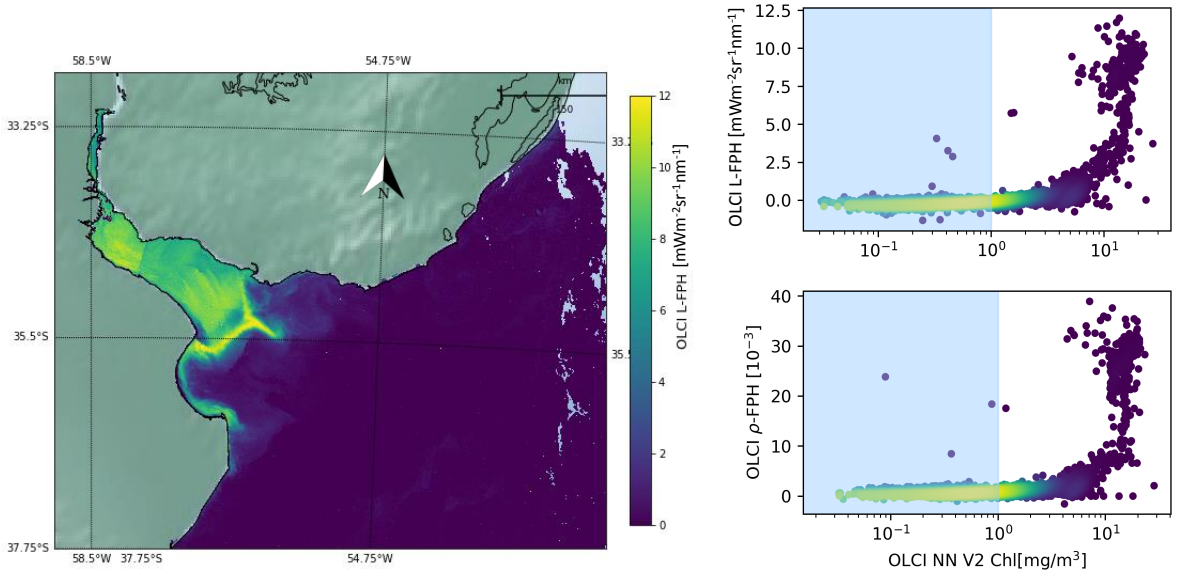

Figure 9. Left: L-FPH from OLCI on the 26th of November, 2017 in the Rio de la Plata Estuary. Right: L-FPH (upper panel) and ρ_w-FPH (lower panel) against chlorophyll from NN V2 in the Rio de la Plata Delta.

As an example of extreme complex water, we examine the Rio de la Plata Estuary. The South Atlantic Ocean near the Rio de la Plata Estuary is a highly dynamic and complex region that encompasses both Case 1 and Case 2 water types. The head of the estuary is characterized by a well-developed turbidity front. High turbidity constrains photosynthesis. Immediately offshore the turbidity front, water becomes less turbid and phytoplankton peaks [40]. Figure 9 shows the L-FPH retrieved in this region on the 26th of November, 2017. There is a strong gradient from the delta to the open ocean and the fluorescence peaks along a front, which is apparently the reported turbidity front.

For the pixel-wise comparison of FPH and chlorophyll in the Rio de la Plata delta we apply the C2RCC alternate net processor (NN V2) [36], which has been amended by a set of additional neural networks that have been trained to cover extreme ranges of scattering and absorption. This scene is characterized by extremely high, but also very low values of chlorophyll. The concentration estimated by the C2RCC processor reaches from 0.02 mg/m^3 in the open ocean to 25 mg/m^3 in the estuary. We can see a clear correlation, which is flat for low and becoming steep for high chlorophyll values.

 doi:10.20944/preprints202009.0554.v1

3.3. OLCI FPH against MODIS nFLH

Only in the comparison of L-FPH, ρ_w-FPH and MODIS nFLH two fluorescence measures are compared to each other. nFLH from MODIS is a well-established remote sensing product and independent of our OLCI FPH products in terms of instrumental issues as well as in terms of retrieval algorithm issues. The retrieval of MODIS nFLH is described in detail in [12]. In the following we show three examples of a matchup comparison between OLCI and MODIS. The results are collocated by projecting OLCI on MODIS pixels through nearest neighbour sampling. The quantitative comparison is shown in a scatter plot in Figure 10. Both, MODIS nFLH and OLCI L-FPH are based on the physical radiances (the MODIS one has undergone atmospheric correction), where the spectral peak around 682 nm is expected to originate from the ocean. Accordingly both measures are expected to be very similar in absolute values. However, MODIS nFLH algorithm is based on the fully normalized water-leaving radiances, including BRDF correction, as described in [41] and both our OLCI products still include BRDF effects (see Section 1). Also, MODIS nFLH characterizes the line-height of the measured spectrum at 678 nm and OLCI FPH characterizes a peak height of a peak centered at 682.5 nm, taking into account the overlaying absorption dip centered at 673.5 nm. The overall patterns of OLCI L-FPH and ρ_w-FPH are so alike that the correlation coefficient to MODIS is in both cases nearly the same. Due to the physical units, absolute values of L-FPH are more comparable to MODIS, than the ones of ρ_w-FPH, while the negative offset of ρ_w-FPH is more comparable to MODIS, than the one from L-FPH. This is most likely due to the atmospheric correction, which is applied as well to MODIS L_w^N as to OLCI ρ_w. The correlation is very good for the Barents Sea and the German Bight example and less good for the Namibian coast, where the time gap of 4h is probably to large.

Preprints (www.preprints.org) | NOT PEER-REVIEWED | Posted: 23 September 2020 doi:10.20944/preprints202009.0554.v1

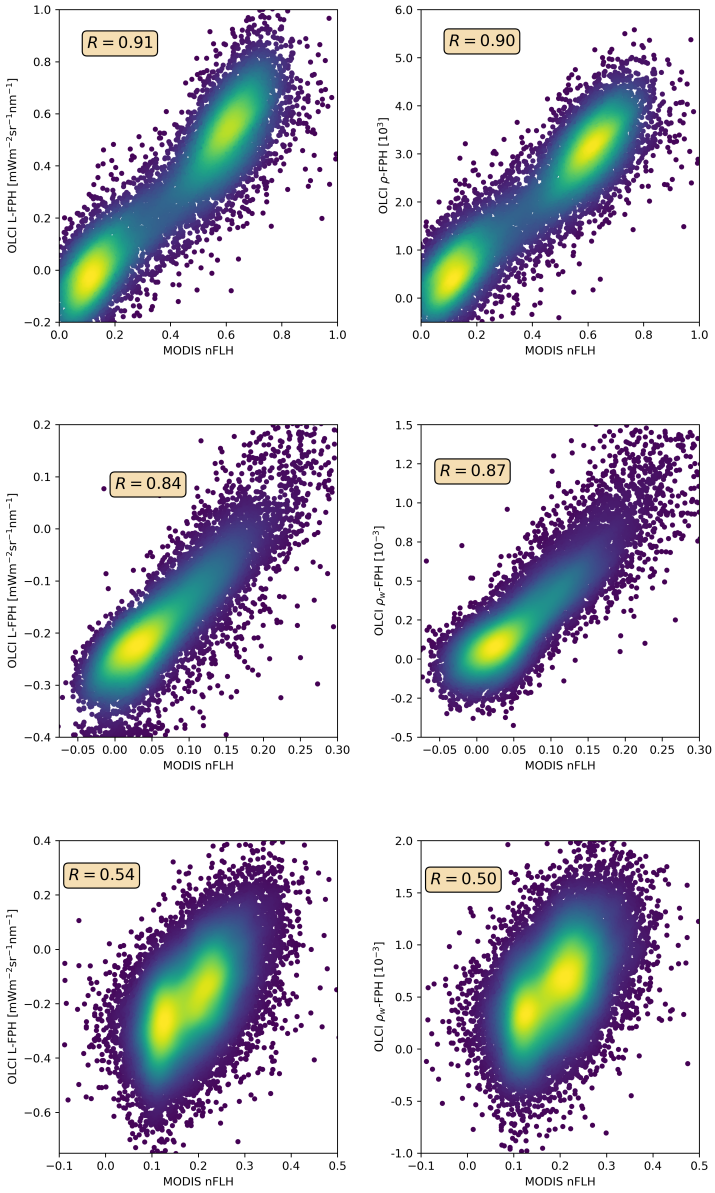

Figure 10. MODIS nFLH over OLCI L-FPH (left) and MODIS nFLH over OLCI ρ_w-FPH (right) in the Barents Sea (upper panel), the German Bight (middle panel) and the Namibian coast (lower panel).

Preprints (www.preprints.org) | NOT PEER-REVIEWED | Posted: 23 September 2020 doi:10.20944/preprints202009.0554.v1

3.4. FPH from Simulated Data

Finally L-FPH and ρ_w-FPH are compared to the input chlorophyll from RTM simulations. Radiative transfer simulations of synthetic L_{TOA} and ρ_w spectra were performed for the development and evaluation of the OC-Fluo algorithm. As described before, the emitted fluorescence quantum in nature depends on many factors, like the quantum yield, the chlorophyll concentration, illumination, etc., which are not known, or at least not accurately known. A synthetic approach, like the one described here is the only way to control all influences on the fluorescence signal. In the RTM fluorescence is a strictly increasing function of the chlorophyll concentration. In case the mathematical function is able to capture the fluorescence peak from OLCI spectrally convoluted reflectances the retrieved FPH should be a strictly increasing function to input chlorophyll.

The simulations are performed using the vector version of MOMO ([42], [43]). Here a horizontal homogeneous atmosphere and ocean consisting of layers with vertical uniform optical properties are assumed. The upward and downward directed light field is calculated at all inter-layer boundaries and for all solar positions. The azimuthal dependence of the light field is internally expressed as Fourier series and reconstructed at equidistant distributed azimuth angles. For this set of simulations a water body was implemented with 20 layers of 1m thickness and is assumed to be homogeneous with an equal distribution of constituents (phytoplankton and CDOM) in each layer. We apply a bio-optical model, where chlorophyll concentration governs as well chlorophyll absorption coupled to chlorophyll fluorescence with a quantum yield of 0.03, as CDOM absorption and scattering ([44]). The chlorophyll-a extinction coefficient and the corresponding single scattering albedo control the amplitude and spectral signature of phytoplankton. A normalized chlorophyll-a absorption spectrum is scaled at 440 nm in order to calculate the absorption spectrum $a_{ph}(\lambda)$ for different phytoplankton amounts. The single scattering albedo ω_0 at 440 nm is set to 0.68 to calculate spectral phytoplankton scattering $b_{ph}(\lambda)$ with

$$b_{ph}(\lambda) = a_{ph}(\lambda)\omega_0\lambda/(1-\omega_0) \tag{20}$$

Phytoplankton scattering is constrained by a phase function measured from [45] which can be mathematically expressed with the Fournier-Forand function with a backscattering ratio of 0.01986. The simulated data cover a large range of chlorophyll concentrations (see table 2), which are governed by the absorption coefficients at 440 nm from 0.04 m^{-1} to 7 m^{-1}. The simulations are performed in 1 nm resolution from 390 nm to 740 nm.

Technically the fluorescence is simulated in two subsequent model runs. In the first run the energy that is absorbed by chlorophyll (photosynthetically active radiation, PAR) is calculated and in the second model run this energy is multiplied by the quantum efficiency of 0.03 and implemented as a Gaussian shaped peak source, centered at 682.5 nm and halfwidth of 25 nm.

Table 2. Input chlorophyll for the simulations

chl-a absorption @ 440 nm [1/m]	0.04	0.4	0.8	1.0	1.4	1.8	3.0	5.0	7.0
concentration [mg/m^3]	0.84	8.4	16.8	21	29.4	37.8	63	105	147

L_{TOA} is a direct model output, namely the upward radiance (L↑) at the uppermost atmospheric layer. The ρ_w is not a direct model output, but is derived from up- and downward radiances (L↑, L↓) and irradiances (E↑, E↓) just above water surface:

$$\rho_w(\theta,\phi,\lambda) = \pi L_w(\theta,\phi,\lambda)/E\downarrow(\lambda) \tag{21}$$

where the water-leaving radiance L_w is calculated from

$$L_w(\theta,\phi,\lambda) = (L\uparrow(\theta,\phi,\lambda) - L_{black}(\theta,\phi,\lambda))/E\downarrow(\lambda) \tag{22}$$

Preprints (www.preprints.org) | NOT PEER-REVIEWED | Posted: 23 September 2020 doi:10.20944/preprints202009.0554.v1

and L_{black} is L↑ from only the ocean surface. This is realised in the model, by implementing a very thin water body with a black surface below.

L_{TOA} and ρ_w are convoluted using the spectral response functions of OLCI. ρ_w is shown in Figure 11 in 1 nm resolution and in OCLI's spectral resolution within the spectral domain of the OLCI bands Oa8 to Oa12. The MERIS band setting, which is a subset of OLCIS bands is included.

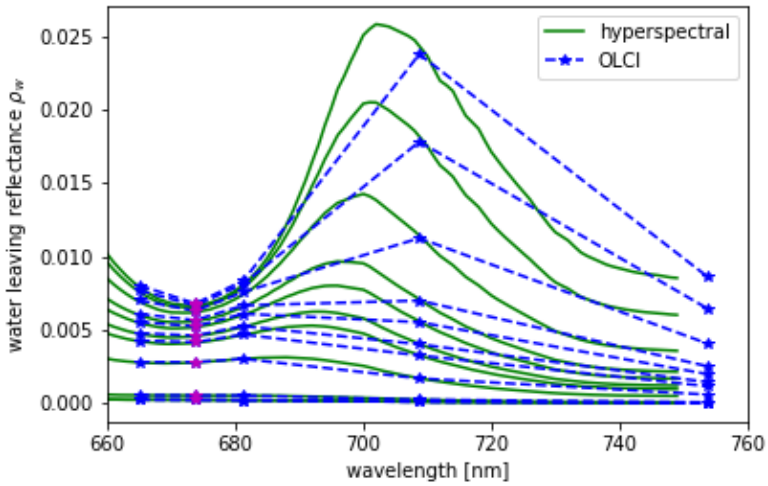

Figure 11. Hyperspectral (green) ρ_w from RTM and its convolution to OLCI (blue) spectral resolution for θ_S=48°, θ_V=34°, ϕ_V=90° and chlorophyll concentrations given in table 2, while the lowest spectrum is the one with the lowest chlorophyll concentration. Band Oa09 from OLCI which is additional to MERIS bands is shown in magenta.

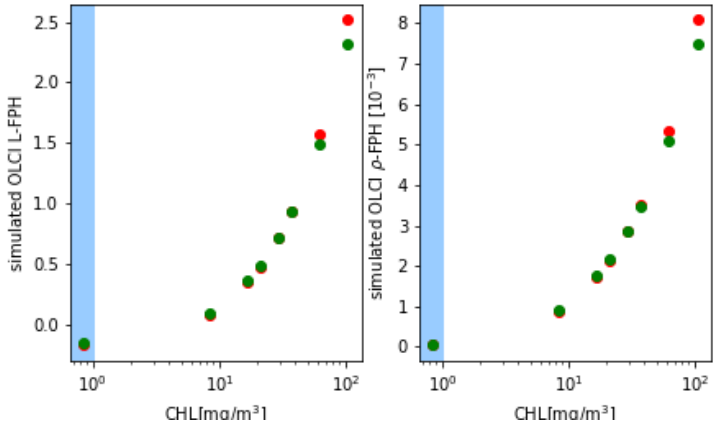

Figure 12. L-FPH (left panel) and ρ_w-FPH (right panel) retrieved from synthetic spectra over chlorophyll, which was input for the RTM for OLCI (green) and for MERIS (red) band setting.

From the synthetic L and ρ_w L-FPH and ρ_w-FPH are retrieved and compared to the input chlorophyll-a concentration. This is shown in Figure 12 for OLCI and MERIS band setting, while the MERIS results are produced by just excluding band Oa9 from the retrieval. Both band settings give an unambigous and very similar relationship. Up to 40 mg/m^3 chlorophyll the difference is less than 4% and even for very high concentrations up to 140 mg/m^3 it does not exceed 10%. In order to investigate the reasons for the similarity of OLCI and MERIS results, we illustrate the extracted spectral components. The division into the spectral components is shown in Figure 13 for OLCI and for only MERIS bands applied to a ρ_w-spectrum with low and with high chlorophyll. For low

Preprints (www.preprints.org) | NOT PEER-REVIEWED | Posted: 23 September 2020 doi:10.20944/preprints202009.0554.v1

chlorophyll concentrations the spectral model seems to reproduce the simulated spectrum perfectly as well for MERIS as for the OLCI band setting. For higher concentrations the additional band Oa9 pulls the reproduced spectrum a bit down, which leads to a slightly lower FPH. The fact that the reproduced spectrum is slightly off the measured bands indicates that for extremely high chlorophyll concentrations the model could be adjusted to a spectrally even more complex behaviour. Figure 14

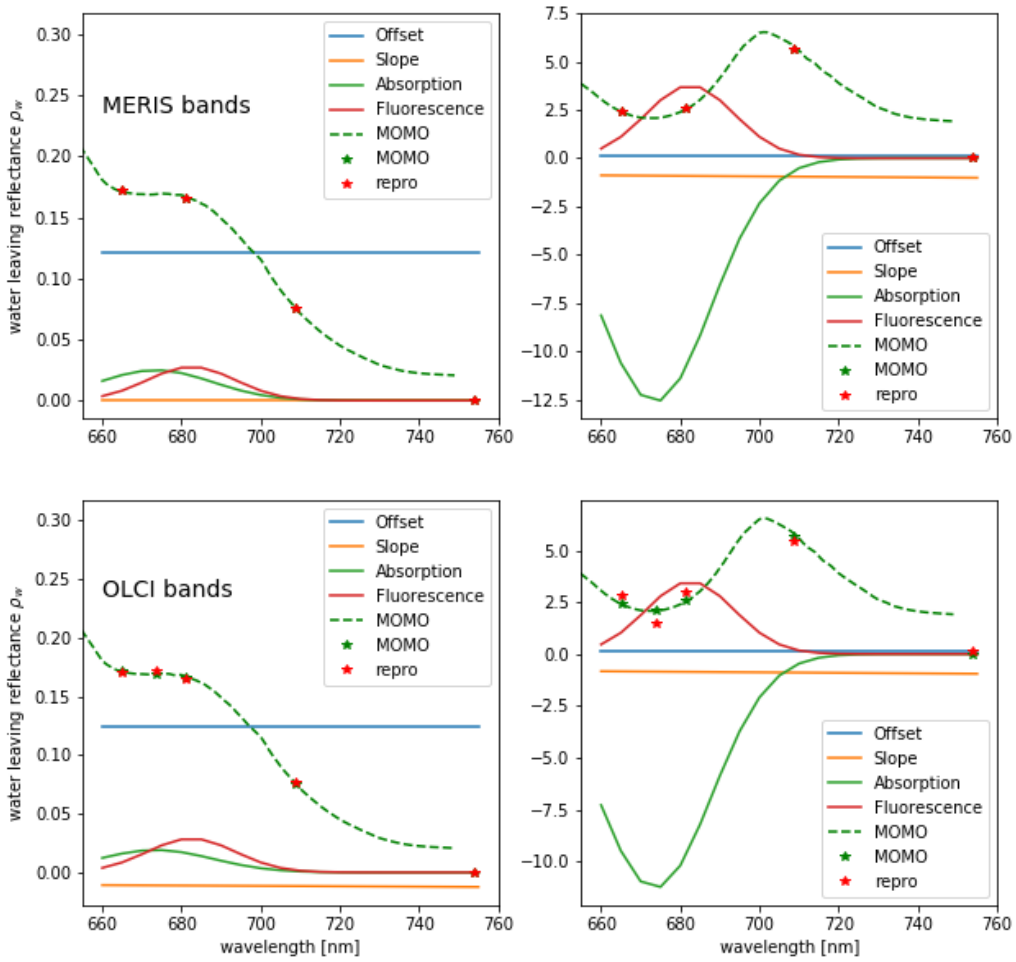

Figure 13. Components found by the retrieval of ρ_w-FPH applied to a ρ_w-spectrum with low (left panels) and with high (right panels) chlorophyll for MERIS (upper panel) and for OLCI (lower panel) band setting.

shows L-FPH retrieved from OLCI measurements over L-FPH retrieved from MERIS measurements and the same for ρ_w-FPH. The correlation is very high and shows that the algorithm could be directly transferred to MERIS data. Finally the results of the RTM exercise, which are shown in Figure 12 are overlaid with the results from the in-situ comparison in Section 3.1 (see Figure 15). Absolute values and slope of the FPH - chlorophyll comparison are very consistent.

Preprints (www.preprints.org) | NOT PEER-REVIEWED | Posted: 23 September 2020 doi:10.20944/preprints202009.0554.v1

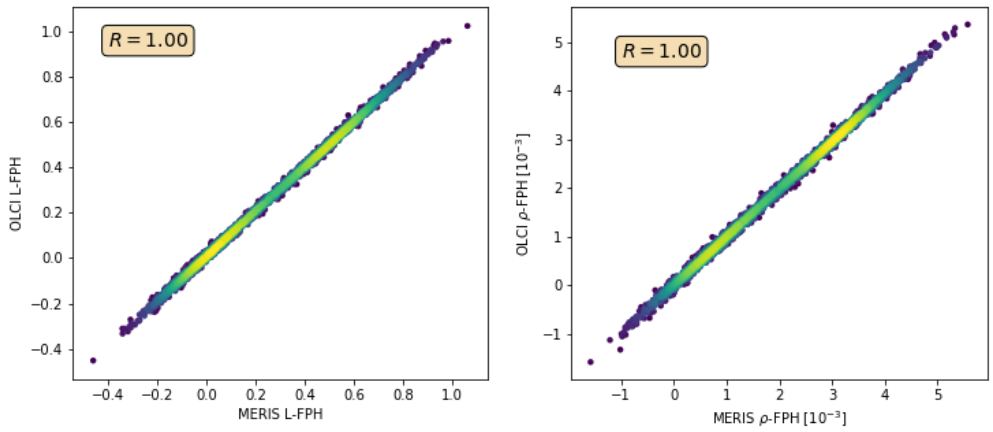

Figure 14. L-FPH retrieved from OLCI measurements over L-FPH retrieved from MERIS measurements (left panel). Same for ρ_w-FPH (right panel)

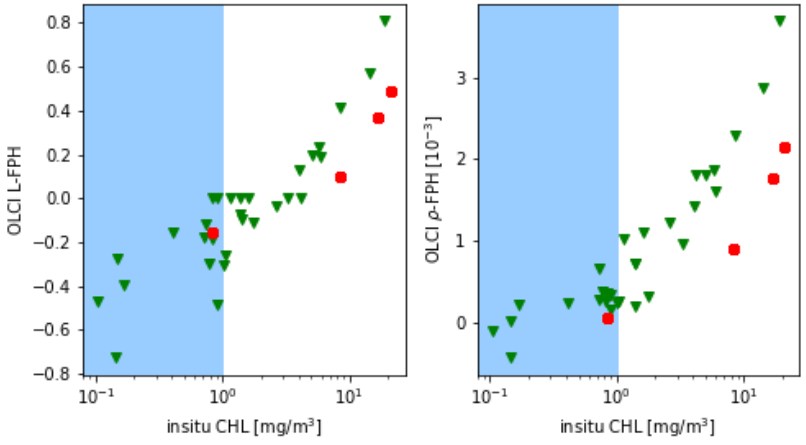

Figure 15. L-FPH (left panel) and ρ_w-FPH (right panel) retrieved from OLCI measurements and simulated spectra over chlorophyll.

 doi:10.20944/preprints202009.0554.v1

4. Discussion and Conclusion

We presented an algorithm that derives the Fluorescence Peak Height (L-FPH and ρ_w-FPH) from spectral radiance satellite data. The algorithm is based on a simple physical model of the spectral absorption and emission in water. The algorithm is applicable on Level-1 data, and therefore, does not depend on atmospheric correction, which is often problematic in complex waters. The technical implementation allows a very fast and stable retrieval.

The new fluorescence algorithm is applied to OLCI Level-1 and Level-2 data and evaluated by a comparison of the retrieved L-FPH and ρ_w-FPH to chlorophyll concentration from various other sources. First, the comparison to in-situ HPLC measurements from a global OLCI matchup database gives a good correlation. Due to more scatter and estimated negative FPH values we define a sensitivity threshold for the algorithm above a concentration of around $1\,\mathrm{mg/m^3}$ chlorophyll. Secondly, the direct comparison to other OLCI standard products like NN and OC4me chlorophyll shows an overall good correlation. Even in complex waters like the Rio de la Plata estuary the correlation between the retrieved L-FPH and ρ_w-FPH to chlorophyll from NN V2 is good. The third part of the evaluation is based on the correlation to MODIS FLH evaluated by means of a matchup comparison in the Barents Sea, the Namibian coast and the German Bight, which gives a nearly linear correlation. A fourth part of the evaluation is based on RTM. Here, synthetic data is processed and the resulting L-FPH and ρ_w-FPH are compared to the used chlorophyll concentration. The resulting relationship between FPH and chlorophyll from the RTM exercise and the in-situ matchup comparison are consistent. The algorithm is applicable to measurements of spectral radiance or reflectance with at least 4 bands in the range between 650 and 750 nm. From RTM we can conclude, that the band setting of OLCIs predecessor MERIS band setting is sufficient to be input to the presented algorithm. This is also tested with real measurements. The consistent application on MERIS data is of special interest in the scope of Ocean Colour (OC), which is recognised as an Essential Climate Variable (ECV) by the Global Climate Observing System (GCOS). With both, MERIS and OLCI observations, a global time series of nearly twenty years of FPH could be generated and analysed.

The additional retrieved chlorophyll absorption at 620 nm (APD) is another parameter of high interest, since chlorophyll absorption is also a good proxy for phytoplankton biomass. This is valid, as well for the maximum absorption in the green spectral range as for the weaker absorption peak in the red. The APD, which is evaluated in the red, is affected in the same way by the specific layering of the phytoplankton as the FPH. But it is not affected in the same way, or not as intensively by phytoplankton species, physiological state or photoinhibition. The combination of APD and FPH can give new insights into the biology, the layering and physiological states of the phytoplankton.

The algorithm as it is assumes a fixed position of the fluorescence peak. However in reality this position can change with phytoplankton species of functional type. For hyperspectral measurements the retrieval may be extended and include more retrieval parameter, e.g. λ_F. The algorithm is implemented and available through SNAP [46] as the plugin "OLCI Fluorescence Processor".

Acknowledgments: We acknowledge EUMETSAT for founding and especially Ewa Kwiatkowska for her substantial support. We thank David Siegel, Toby Westberry, Michael Behrenfeld, Emmanuel Boss, Lynne Talley, Curt Davis, Ajit Subramaniam, Antonio Mannino, Aimee Neeley and Javier Concha for their effort in collecting the data used in this investigation and for making them available for publication. We also thank the EC Copernicus Programme and EUMETSAT for establishing and maintaining the OCDB. We thank the European Commission for founding from the Copernicus Programme and the name/contract-number

Author Contributions: conceptualization, L.K., R.P and J.F.; methodology, L.K. and R.P.; software, L.K. and R.P.; validation, L.K., R.P. and J.F.; formal analysis, L.K.; investigation, L.K., R.P. and J.F.; resources, L.K., ; data curation, L.K. and R.P.; writing—original draft preparation, L.K.; writing—review and editing, L.K.,R.P. and J.F.; visualization, L.K. and R.P.; supervision, L.K., R.P and J.F.; project administration, L.K., R.P and J.F.; funding acquisition, L.K., R.P and J.F.

Conflicts of Interest: The authors declare no conflict of interest. The funders had no role in the design of the study; in the collection, analyses, or interpretation of data; in the writing of the manuscript, or in the decision to publish the results.

1. Craig Donlon. estec Sentinel-3 Mission Requirements Traceability Document (MRTD) - PDF. Technical report, European Space Research and Technology Centre, 2011.
2. Donlon, C.; Berruti, B.; Buongiorno, A.; Ferreira, M.H.; Féménias, P.; Frerick, J.; Goryl, P.; Klein, U.; Laur, H.; Mavrocordatos, C.; Nieke, J.; Rebhan, H.; Seitz, B.; Stroede, J.; Sciarra, R. The Global Monitoring for Environment and Security (GMES) Sentinel-3 mission. *Remote Sensing of Environment* **2012**, *120*, 37–57. doi:10.1016/j.rse.2011.07.024.
3. Odermatt, D.; Gitelson, A.; Brando, V.E.; Schaepman, M. Review of constituent retrieval in optically deep and complex waters from satellite imagery. *Remote Sensing of Environment* **2012**, *118*, 116–126. doi:10.1016/j.rse.2011.11.013.
4. Xing, X.G.; Zhao, D.Z.; Liu, Y.G.; Yang, J.H.; Xiu, P.; Wang, L. An overview of remote sensing of chlorophyll fluorescence. *Ocean Science Journal* **2007**, *42*, 49–59. doi:10.1007/BF03020910.
5. Neville, R.A.; Gower, J.F.R. Passive remote sensing of phytoplankton via chlorophyll α fluorescence. *Journal of Geophysical Research* **2008**, *82*, 3487–3493. doi:10.1029/jc082i024p03487.
6. Babin, M.; Morel, A.; Gentili, B. Remote sensing of sea surface Sun-induced chlorophyll fluorescence: consequences of natural variations in the optical characteristics of phytoplankton and the quantum yield of chlorophyll a fluorescence. *International Journal of Remote Sensing* **1996**, *17*, 2417–2448. doi:10.1080/01431169608948781.
7. Gower, J.; King, S. Use of satellite images of chlorophyll fluorescence to monitor the spring bloom in coastal waters. *International Journal of Remote Sensing* **2012**, *33*, 7469–7481. doi:10.1080/01431161.2012.685979.
8. Falkowski, P.; Kiefer, D.A. Chlorophyll-a fluorescence in phytoplankton: relationship to photosynthesis and biomass. *Journal of Plankton Research* **1985**, *7*, 715–731. doi:10.1093/plankt/7.5.715.
9. Mazeran, C.; Brockmann, C.B.; Ruddick, K.; Voss, K.; Zagolski, F. Requirements for Copernicus Ocean Colour Vicarious Calibration Infrastructure. 2017, number July.
10. Lin, H.; Kuzminov, F.I.; Park, J.; Lee, S.; Falkowski, P.G.; Gorbunov, M.Y. Phytoplankton. The fate of photons absorbed by phytoplankton in the global ocean. *Science (New York, N.Y.)* **2016**, *351*, 264–7. doi:10.1126/science.aab2213.
11. Fischer, J.; Kronfeld, U. Sun-stimulated chlorophyll fluorescence 1: Influence of oceanic properties. *International Journal of Remote Sensing* **1990**, *11*, 2125–2147. doi:10.1080/01431169008955166.
12. Behrenfeld, M.J.; Westberry, T.K.; Boss, E.S.; O'Malley, R.T.; Siegel, D.A.; Wiggert, J.D.; Franz, B.A.; McClain, C.R.; Feldman, G.C.; Doney, S.C.; Moore, J.K.; Dall'Olmo, G.; Milligan, A.J.; Lima, I.; Mahowald, N. Satellite-detected fluorescence reveals global physiology of ocean phytoplankton. *Biogeosciences* **2009**, *6*, 779–794. doi:10.5194/bg-6-779-2009.
13. Gower, J.; King, S. Validation of chlorophyll fluorescence derived from MERIS on the west coast of Canada. *International Journal of Remote Sensing* **2007**, *28*, 625–635. doi:10.1080/01431160600821010.
14. Gower, J.; King, S. Validation of chlorophyll fluorescence derived from MERIS on the west coast of Canada. *International Journal of Remote Sensing* **2007**, *28*, 625–635. doi:10.1080/01431160600821010.
15. Gordon, H.R.; Voss, K.J. MODIS Normalized Water-leaving Radiance Algorithm Theoretical Basis Document (MOD 18). Technical Report Mod 18, Department of Physics, University of Miami, 1999.
16. Hoge, F.E.; Lyon, P.E.; Swift, R.N.; Yungel, J.K.; Abbott, M.R.; Letelier, R.M.; Esaias, W.E. Validation of Terra-MODIS phytoplankton chlorophyll fluorescence line height I Initial airborne lidar results. *Applied Optics* **2003**, *42*, 2767. doi:10.1364/AO.42.002767.
17. Huot, Y.; Brown, C.A.; Cullen, J.J. New algorithms for MODIS sun-induced chlorophyll fluorescence and a comparison with present data products. *Limnology and Oceanography: Methods* **2005**, *3*, 108–130. doi:10.4319/lom.2005.3.108.
18. Moreno-Madriñán, M.J.; Fischer, A.M. Performance of the MODIS FLH algorithm in estuarine waters: a multi-year (2003–2010) analysis from Tampa Bay, Florida (USA). *International Journal of Remote Sensing* **2013**, *34*, 6467–6483. doi:10.1080/01431161.2013.804227.

19. Carder, K.L.; Chen, F.R.; Lee, Z.; Hawes, S.K.; Cannizzaro, J.P. ATBD 19, Case 2 Chlorophyll a. Technical report, University of South Florida, College of Marine Science, 2003.
20. Gons, H.; Auer, M.; of Environment, S.E.R.S.; 2008, U. MERIS satellite chlorophyll mapping of oligotrophic and eutrophic waters in the Laurentian Great Lakes. *Elsevier* **2008**.
21. Letelier, R. An analysis of chlorophyll fluorescence algorithms for the moderate resolution imaging spectrometer (MODIS). *Remote Sensing of Environment* **1996**, *58*, 215–223. doi:10.1016/S0034-4257(96)00073-9.
22. Binding, C.E.; Greenberg, T.A.; Jerome, J.H.; Bukata, R.P.; Letourneau, G. An assessment of MERIS algal products during an intense bloom in Lake of the Woods. *Journal of Plankton Research* **2011**, *33*, 793–806. doi:10.1093/plankt/fbq133.
23. Ioannou, I.; Zhou, J.; Gilerson, A.; Gross, B.; Moshary, F.; Ahmed, S. New algorithm for MODIS chlorophyll fluorescence height retrieval: performance and comparison with the current product. 2009, p. 747309. doi:10.1117/12.830630.
24. Kiefer, D.A. Fluorescence properties of natural phytoplankton populations. *Marine Biology* **1973**, *22*, 263–269. doi:10.1007/BF00389180.
25. Hu, C.; Muller-Karger, F.E.; Taylor, C.J.; Carder, K.L.; Kelble, C.; Johns, E.; Heil, C.A. Red tide detection and tracing using MODIS fluorescence data: A regional example in SW Florida coastal waters. *Remote Sensing of Environment* **2005**, *97*, 311–321. doi:10.1016/J.RSE.2005.05.013.
26. Wolanin, A.; Rozanov, V.; Dinter, T.; Noël, S.; Vountas, M.; Burrows, J.; Bracher, A. Global retrieval of marine and terrestrial chlorophyll fluorescence at its red peak using hyperspectral top of atmosphere radiance measurements: Feasibility study and first results. *Remote Sensing of Environment* **2015**, *166*, 243–261. doi:10.1016/J.RSE.2015.05.018.
27. Erickson, Z.K.; Frankenberg, C.; Thompson, D.R.; Thompson, A.F.; Gierach, M. Remote Sensing of Chlorophyll Fluorescence in the Ocean Using Imaging Spectrometry: Toward a Vertical Profile of Fluorescence. *Geophysical Research Letters* **2019**, *46*, 1571–1579. doi:10.1029/2018GL081273.
28. Ruddick, Kevin George, Ovidio, Fabrice and Rijkeboer, M.; The. Atmospheric correction of Sea WiFS imagery for turbid coastal and inland waters. *Applied Optics* **2000**, *39*, 897–912. doi:10.1364/AO.39.000897.
29. Bourg, L.; Vincent, E.; Muguet, I. OLCI Level 2 Algorithm Theoretical Basis Document, 2010.
30. Platt, U.; Perner, D. Measurements of Atmospheric Trace Gases by Long Path Differential UV/Visible Absorption Spectroscopy. *Optical and Laser Remote Sensing* **1983**, *39*, pp 97–105. doi:https://doi.org/10.1007/978-3-540-39552-2_13.
31. Fischer, J.; Preusker, R.; Lindstrot, R. Correction of the impact of the absorption of atmospheric gases - OLCI Level 2 Algorithm Theoretical Basis Document **2010**. pp. 1–37.
32. Rodgers, C.D. *Inverse Methods for Atmospheric Sounding: Theory and Practice.*; World Scientific., 2000.
33. Vincent, E.; Muguet, I. Level 2 Algorithm Theoretical Basis Document Instrumental Corrections OLCI. Technical report, 2010.
34. Doppler, L.; Preusker, R.; Bennartz, R.; Fischer, J. K-bin and k-IR: K-distribution methods without correlation approximation for non-fixed instrument response function and extension to the thermal infrared-Applications to satellite remote sensing. *Journal of Quantitative Spectroscopy and Radiative Transfer* **2014**, *133*, 382–395. doi:10.1016/j.jqsrt.2013.09.001.
35. Morel, A.; Gentili, B.; Claustre, H.; Babin, M.; Bricaud, A.; Ras, J.; Tièche, F. Optical properties of the "clearest" natural waters. *Limnology and Oceanography* **2007**, *52*, 217–229. doi:10.4319/lo.2007.52.1.0217.
36. Brockmann, C.; Doerffer, R.; Marco, P.; Stelzer, K.; Embacher, S.; Ruescas, A. Evolution Of The C2RCC Neural Network For Sentinel 2 and 3 For The Retrieval of Ocean. *Proc. 'Living Planet Symposium 2016', Prague, Czech Republic, 9–13 May 2016 (ESA SP-740, August 2016)* **2016**, *2016*, 9–13.
37. Werdell, P.J.; Bailey, S.; Fargion, G.; Pietras, C.; Knobelspiesse, K.; Feidman, G.; Mcclain, C. Unique data repository facilitates ocean color satellite validation. *Eos* **2003**, *84*, 2002–2004. doi:10.1029/2003EO380001.
38. Eumetsat. Ocean Colour In-Situ Database, 2019.
39. EUMETSAT. Recommendations for Sentinel-3 OLCI Ocean Colour product validations in comparison with in situ measurements – Matchup Protocols. Technical report, 2019.
40. Marcelo Acha, E.; Mianzan, H.; Guerrero, R.; Carreto, J.; Giberto, D.; Montoya, N.; Carignan, M. An overview of physical and ecological processes in the Rio de la Plata Estuary. *Continental Shelf Research* **2008**, *28*, 1579–1588. doi:10.1016/j.csr.2007.01.031.

41. Feldman, G.C. NASA's OceanColor Web.
42. Fell, F.; Fischer, J. Numerical simulation of the light field in the atmosphere-ocean system using the matrix-operator method. *Journal of Quantitative Spectroscopy and Radiative Transfer* **2001**, *69*, 351–388. doi:10.1016/S0022-4073(00)00089-3.
43. Hollstein, A.; Fischer, J. Radiative transfer solutions for coupled atmosphere ocean systems using the matrix operator technique. *Journal of Quantitative Spectroscopy and Radiative Transfer* **2012**, *113*, 536–548. doi:10.1016/j.jqsrt.2012.01.010.
44. Bricaud, A.; Babin, M.; Claustre, H.; Ras, J.; Tièche, F. Light absorption properties and absorption budget of Southeast Pacific waters. *Journal of Geophysical Research: Oceans* **2010**, *115*, 1–19. doi:10.1029/2009JC005517.
45. Petzold, T. Volume Scattering Functions for Selected Ocean Waters. *Scripps Inst. Oceanogr.* **1972**, pp. SIO Ref. 72–78, [arXiv:physics/0608246]. doi:10.5811/westjem.2013.7.18472.
46. Http://step.esa.int. SNAP - ESA Sentinel Application Platform v7.0.3.